Electron collisions with CO molecule: Potential energy curves of higher lying CO^- resonant states

Amar Dora[1] **and Jonathan Tennyson**[2]

[1]Department of Chemistry, North Orissa University, Baripada 757003, Odisha, India
[2]Department of Physics and Astronomy, University College London, Gower St., London WC1E 6BT, UK

E-mail: amardora@gmail.com and j.tennyson@ucl.ac.uk

Abstract.

Resonance energies and widths of eight long-lived metastable electronic states of the CO^- anion are obtained using the **R**-matrix method as a function of bond distance. High-level *ab-initio* scattering calculations are performed for a large number (above 150) of fixed-nuclear geometries using the large cc-pV6Z Gaussian basis set and a close-coupling model involving 27 low-lying target states. Potential curves for narrow resonances, three $^2\Sigma^+$, four $^2\Pi$ and one $^2\Delta$, in the 10 – 14 eV region are reported, along with the data on the low-lying $^2\Pi$ shape resonance. These curves provide a starting point for performing nuclear dynamics and hence studies of dissociative attachment via these states.

1. Introduction

There has been a long history of studies of electron-collision resonances in the CO molecule (Schulz 1973, Mazeau et al. 1975, Wallbank et al. 1983, Olszewski et al. 1998). At low energies the CO $^2\Pi$ shape resonance at 1.6 eV is well known and found to lead to complicated structures in the observed cross sections (Haddad & Milloy 1983, Allan 1989, Gibson et al. 1996, Poparić et al. 2006, Allan 2010) which result in significant enhancements in the vibrational excitation cross sections (Campbell et al. 2011, Laporta et al. 2012). At higher energies (10 – 14 eV) studies have pointed towards a number of narrow resonances associated with the excited (Rydberg-like) electronic states of the CO molecule in this region (Mazeau et al. 1975, Wallbank et al. 1983, Newman et al. 1983, Polley & Bailey 1988, Middleton et al. 1993, Olszewski et al. 1998). However, there has been little consensus between these studies over the nature or, indeed, number of the resonances.

These higher-lying resonances have also been extensively probed in dissociative electron attachment (DEA) experiments. These experiments monitor the C^- or O^- anions produced as result of an electron collision (Rapp & Briglia 1965, Chantry 1968, Stamatovic & Schulz 1970, Cadex et al. 1975, Hall et al. 1977, Nag & Nandi 2015*b*), a process that only occurs via a resonance (Fabrikant et al. 2017). The observed DEA cross sections show a broad peak in the 9 to 12 eV energy range. Sanche & Schulz (1971) identified a $^2\Sigma^+$ resonance at 10.04 eV which is assumed to contribute to this DEA peak. Furthermore, shape resonances at 10.4 eV and 10.7 eV and Feshbach resonances at 11.3 eV and 12.2 eV were reported from experiments (Schulz 1973, Sanche & Schulz 1971, Mazeau et al. 1972); these may also contribute to DEA.

DEA studies show that O^- ion production is generally favoured and the cross section for C^- production is small. Recent experiments have used velocity time sliced imaging as a method of probing the nature of these resonances through the measurement of O^- angular distributions (Nag & Nandi 2015*b*, Tian et al. 2013, Wang et al. 2015). However, these studies arrived at different conclusions from analysing their results. **?** claimed to observe complete backward scattering of O^- fragments and through their analysis using an axial recoil approximation model, they proposed that DEA at 10.6 eV proceeds through a coherent superposition of $^2\Pi$, $^2\Delta$, and $^2\Phi$ resonant states of CO^-. However, **?**, who used a similar experimental setup to that used by Tian *et al* , question the above claim since they observed forward-backward asymmetry in their measurements of O^- ion angular distribution. Using the same axial recoil approximation model, Nag and Nandi found that they could satisfactorily fit their data in terms of the more standard interference between different partial waves as opposed to the coherent superposition of different resonant states. The newer and more precise measurements made by Gope et al. (2016) obtained results in close agreement to that of Nag and Nandi, which helped to settle the above controversy in favour of interference between different partial waves. However, theoretical calculations should be able to confirm the nature of the resonance(s) involved in this process.

A number of theoretical studies have identified resonances in the higher energy region. These include R-matrix calculations by Salvini et al. (1984), who found a $^2\Sigma^+$ shape resonance at about 20 eV, and by Morgan & Tennyson (1993), who found a rather broad (width, $\Gamma > 1$ eV) resonance for each of the $^2\Sigma^+$, $^2\Pi$ and $^2\Delta$ symmetries they considered. Weatherford & Huo (1990) found 4 resonances in the 10 - 20 eV region based on a two-state calculation. Finally, Pearson & Lefebvre-Brion (1976) used the stabilization method to study continuum states of CO^-; they identified a single, narrow $^2\Sigma^+$ symmetry resonance at 10.2 eV which corresponds with that observed by Sanche & Schulz (1971). More recently we (Dora et al. 2016, Dora & Tennyson 2019) have attempted to address this problem by performing R-matrix calculations using extended basis sets to represent the CO target and 27 CO target states in the close-coupling (CC) expansion. Our first study (Dora et al. 2016) used both cc-pVDZ and a cc-pVTZ Gaussian type orbital (GTO) target basis set and up to 50 state in the close-coupling (CC) expansion. The cc-pVDZ calculations did not recover any resonances above 10 eV while the cc-pVTZ ones found a narrow $^2\Sigma^+$ resonance associated with the b $^3\Sigma^+$ excited ("parent") target state. We concluded that to make progress on this problem we needed to further expand the basis set used to represent the target. So, in a preliminary study for the present work (Dora & Tennyson 2019), we tested a number of target representations and scattering models for CO at its equilibrium geometry. A calculation based on the use of cc-pV6Z GTO basis for the target found several narrow resonances, three $^2\Sigma^+$, one $^2\Pi$ and one $^2\Delta$, in the 10 to 13 eV range. These calculations form the starting point for the present work.

In this paper we present resonance energies and associated widths for CO anion states below 15 eV. These curves are used to identify parent states for the resonances and provide the necessary input for future DEA calculations.

2. Theory and calculation

Before starting scattering calculations it is necessary to perform calculations on the CO molecule to obtain target wavefunctions and energies, and target orbitals which form part of the input for the scattering calculation. Large numbers of target calculations were performed using the Molpro electronic structure code (Werner et al. 2012). Calculations were performed at the complete active space self-consistent-field (CASSCF) level generally using state-averaging (SA-CASSCF). These calculations performed well in the region of the CO equilibrium geometry and in the asymptotic (dissociative) region but gave many difficulties at intermediate internuclear separations. In general these problems were caused by crossings both between individual potential curves which, for instance, caused them to move into and out of the chosen set of curves, and by the exchange of orbitals between those included in the active space and those not. Attempts to mitigate these problems by, for example, rotating the orbitals between different spaces (frozen, valence, virtual) to stop sharp exchanges and starting each calculation from the neighbouring geometry were only partially successful. In the end these issues forced us

to limit the range of geometries for which we attempted to compute resonance curves.

For the scattering calculations we use the **R**-matrix method as implemented in the UK molecular R-matrix codes (UKRmol) (Morgan et al. 1998, Carr et al. 2012). A newer and upgraded version of the codes, called as UKRmol+ (Mašín et al. 2020), became available as the current calculations were nearing completion. UKRmol+ can be used to study larger molecules, molecules at longer bond lengths and, pertinent to the present study, molecules with very diffuse target wavefunctions (Meltzer et al. 2020). Below, we give a brief discussion of the method; the details of the principles involved can be found in the review article by Tennyson (2010).

In the **R**-matrix method the space around electron+target system is separated by an imaginary sphere of certain radius a. The size of the sphere is taken large enough so that all the N-electron target states have zero amplitude at the boundary. Inside the sphere, the $N+1$-electron scattering wavefunction ψ_k^{N+1} is represented by a close-coupling (CC) expansion using the target states Φ_i^N

$$\psi_k^{N+1} = \mathcal{A}\sum_{ij} a_{ijk}\Phi_i^N(\mathbf{x}_1...\mathbf{x}_N)u_{ij}(\mathbf{x}_{N+1}) + \sum_i b_{ik}\chi_i^{N+1}(\mathbf{x}_1...\mathbf{x}_{N+1}). \qquad (1)$$

Here, u_{ij} are the continuum orbitals representing the scattering electron and $\mathcal{A}$ is the anti-symmetrization operator. The χ_i^{N+1}, called L^2 configurations, are obtained by putting all $N+1$ electrons in target molecular orbitals (MOs). These L^2 configurations are used to represent the scattering system at short range. At long range, outside the sphere, the outgoing electron is treated as interacting only with the multipolar potential field of the target molecule. The variational parameters a_{ijk} and b_{ik} are obtained from the diagonalization of the scattering Hamiltonian and are used in evaluating the **R**-matrix at the sphere boundary. The propagation of the **R**-matrix to large distances and matching with asymptotic solutions yields the K-matrix.

The eigenvalues of the K-matrix are related to the eigenphase sum; the later quantities can be fitted to a Breit-Wigner function to obtain the resonance parameters. In this work we have used this method as well as visual inspection of eigenphase sums and cross sections to find and fit the resonances in CO molecule as a function of geometry. As will be seen, most resonances lie very close to their parent target state which complicates the task of extracting resonance parameters.

Both, Molpro and the UKRmol codes cannot use the natural $C_{\infty v}$ symmetry of the CO molecule. Therefore, these calculations were performed using the reduced C_{2v} point group. Since, there are clear correlations linking electronic states between these two point groups, we report target and resonant states using $C_{\infty v}$ symmetry.

In this work we employ the largest compact basis set cc-pV6Z that Molpro can currently support. The need of such a large basis set was shown to be essential for representing the higher energy resonances in our previous work (Dora & Tennyson 2019) on electron–CO collisions at equilibrium geometry. The aug-cc-pV6Z basis set, which includes extra diffuse functions and so is better capable of representing higher lying resonances, was not employed as these basis functions tend to extend outside the R-matrix sphere, particularly at long internuclear separations. We note that a known

consequence of the target basis leaking outside the box is the appearance of spurious extra resonances (Gorfinkiel et al. 2002). Use of such a diffuse basis sets therefore requires larger, possibly much larger, **R**-matrix sphere size which leads to problems both with linear dependence in the continuum basis and greatly increased computational time. Such calculations were deemed impractical at the present time.

2.1. Target calculation

The target molecular orbitals used in scattering calculations were obtained from Molpro SA-CASSCF calculations with the active space configuration defined as: $(1a_1 - 2a_1)^4\,(3a_1 - 6a_1, 1b_1 - 3b_1, 1b_2 - 3b_2)^{10}$. We use the LQUANT option available in the Molpro CASSCF program to specify the L_z quantum number and hence obtained the target states in $C_{\infty v}$ symmetry. A total of 27 low lying states of CO molecule are computed in $C_{\infty v}$ symmetry. These are: 4 $^1\Sigma^+$, 2 $^1\Sigma^-$, 5 $^1\Pi$, 2 $^1\Delta$, 4 $^3\Sigma^+$, 3 $^3\Sigma^-$, 5 $^3\Pi$ and 2 $^3\Delta$. Counting the degenerate states of Π and Δ states separately, this amounts to 41 target states in C_{2v} symmetry.

Initially, the CASSCF potential energy curves (PECs) of the above 27 target states were computed for internuclear bond distance R in the range of $1.5 \leq R \leq 4$ a_0 on a fine grid of 0.001 a_0. However, due to the difficulties associated with representation of higher-lying excited states and the multitude of avoided crossings among them, there were convergence problems at several geometries beyond $R = 2.388$ a_0. Therefore, we present the PECs of the above 27 states of CO molecule for $R \leq 2.388$ a_0. The scattering calculations are also limited for $R \leq 2.388$ a_0 for the above reason.

2.2. Scattering calculation

The **R**-matrix calculations have been performed for a total of 167 geometries comprising of 137 points in the R range of 1.7 a_0 to 2.38 a_0 on a closely spaced grid of 0.005 a_0 and at some additional nearby geometries where the calculations failed to fit resonances at the above chosen grid points. For the lowest $^2\Pi$ resonance we tried calculations extended up to $R = 3.0$ a_0, but the resonance positions obtained did not behave smoothly beyond $R = 2.5$ a_0 due to the above mentioned problems associated with excited target states. The required target molecular orbitals for scattering calculations are taken from the saved target SA-CASSCF calculations described above which was performed for a finer R grid of 0.001 a_0. Our preliminary investigations with cc-pV6Z basis set using both $a = 12a_0$ and larger sphere size of 15 a_0 for the equilibrium geometry of CO showed little difference in the results. In particular the two calculations identified the same number of resonances with those computed using the larger sphere lying just slightly higher in energy, which we attributed to the less complete representation of the continuum in this calculation. For reasons of computation resources and completeness of the continuum basis we used the medium sphere defined by $a = 12$ a_0 for all scattering calculations presented here. This finding is in line with our previous studies on larger molecules (Dora et al. 2009).

The appropriate continuum molecular orbitals for this sphere size are obtained by partial wave expansion up to $\ell \leq 4$ which are represented by Gaussian-type functions (Faure et al. 2002). Higher partial waves are known to be important to converge cross sections at the energies studied, see Zawadzki et al. (2020) for discussion of this. However, the resonances are essentially short-ranged in nature and in this region the high ℓ behaviour is generally modelled by allowing the electron to enter unoccupied target orbitals. We therefore do not expect truncation of the partial wave expansion at g waves to have a significant impact on the resonance parameters. We note that the newly-developed UKRmol+ code (Mašín et al. 2020) allows calculations to be performed with larger partial wave expansions. However, such calculations become computationally very demanding even for a molecule like H_2 (Meltzer et al. 2020), and are currently not feasible with the large target basis set required for the present study.

The scattering wavefunction in the inner region is represented by close-coupling expansion by using the above mentioned 27 target states. The **R**-matrix calculated at the boundary of the sphere were propagated to a distance of 100 a_0 in order to match to the asymptotic analytic functions. We note that this model has also been used as part of a joint experimental – theoretical study on differential cross sections for electron impact electronic excitation of CO (Zawadzki et al. 2020). The agreement between theory and experiment shown by this study was very good for the energy region considered here, which helps to validate our model.

3. Results and discussion

3.1. Target PECs

Table 1 compares our calculated adiabatic electronic excitation energy, usually denoted T_e, with the available experimental values. In general the agreement is good. Given that the resonances discussed below can all be associated with parent target states, the difference between the observed and calculated positions of the target states gives a measure of the uncertainty in our calculated resonance positions. The Figure 1 shows all the 27 target potential energy curves used in the close coupling expansion of scattering wavefunctions in the R-matrix calculations.

3.2. Resonances

Beside the well-known, low-lying and broad $^2\Pi$ shape resonance, our calculations find eight other resonances, three with $^2\Sigma^+$ symmetry, one of $^2\Delta$ symmetry and a further four $^2\Pi$ symmetry resonances. These resonances are all narrow lie in the 10 – 13 eV region; not all the resonances were detected at all geometries and in particular the 2 $^2\Pi$, 3 $^2\Pi$ and 5 $^2\Pi$ resonances were only detected for $R \leq 2$ a_0 and are therefore not found at the CO equilibrium geometry. Table 2 presents a summary of these resonances while Figs. 2 and 3 show their behaviour as a function of internuclear separation.

Table 1. Comparison of vertical excitation energies (in eV) and ground state dipole moments (μ in D) for CO calculated using SA-CASSCF with a cc-pV6Z basis set (Calc.) and experimental values Nielsen et al. (1980).

State	Calc.	Expt.
$X\,^1\Sigma^+$	0.00	0.00
$a\,^3\Pi$	6.43	6.32
$a'\,^3\Sigma^+$	8.36	8.51
$A\,^1\Pi$	8.97	8.51
$d\,^3\Delta$	9.22	9.36
$e\,^3\Sigma^-$	9.60	9.88
$I\,^1\Sigma^-$	9.95	9.88
$D\,^1\Delta$	10.00	10.23
$b\,^3\Sigma^+$	10.39	10.40
$B\,^1\Sigma^+$	11.16	10.78
$2\,^3\Pi$	11.34	
$2\,^1\Pi$	11.84	
$3\,^3\Pi$	12.32	
$4\,^3\Pi$	13.17	
$3\,^1\Pi$	13.38	
$4\,^1\Pi$	13.99	
$3\,^3\Sigma^+$	14.25	
$2\,^3\Delta$	14.40	
$2\,^1\Delta$	14.44	
$2\,^1\Sigma^-$	14.54	
$2\,^3\Sigma^-$	14.55	
$5\,^3\Pi$	14.82	
$3\,^1\Sigma^+$	14.93	
$3\,^3\Sigma^-$	15.42	
$4\,^1\Sigma^+$	15.58	
$4\,^3\Sigma^+$	15.88	
$5\,^1\Pi$	17.12	
μ	0.238	0.122

It is common to associate Feshbach resonances with a particular excited state of the target which is usually described as the parent state. Figures 2 and 3 show that the narrow resonances do indeed all behave as if they are weakly bound to one or more of the CO excited states. These resonances can therefore all be classified as Feshbach in nature. Table 2 identifies parent states for each of these resonances. It can be seen that for some of the resonances more than one parent states is given. The $^2\Delta$ resonance is found to follow both the $4\,^3\Pi$ and $3\,^1\Pi$ states. These states are nearly degenerate with

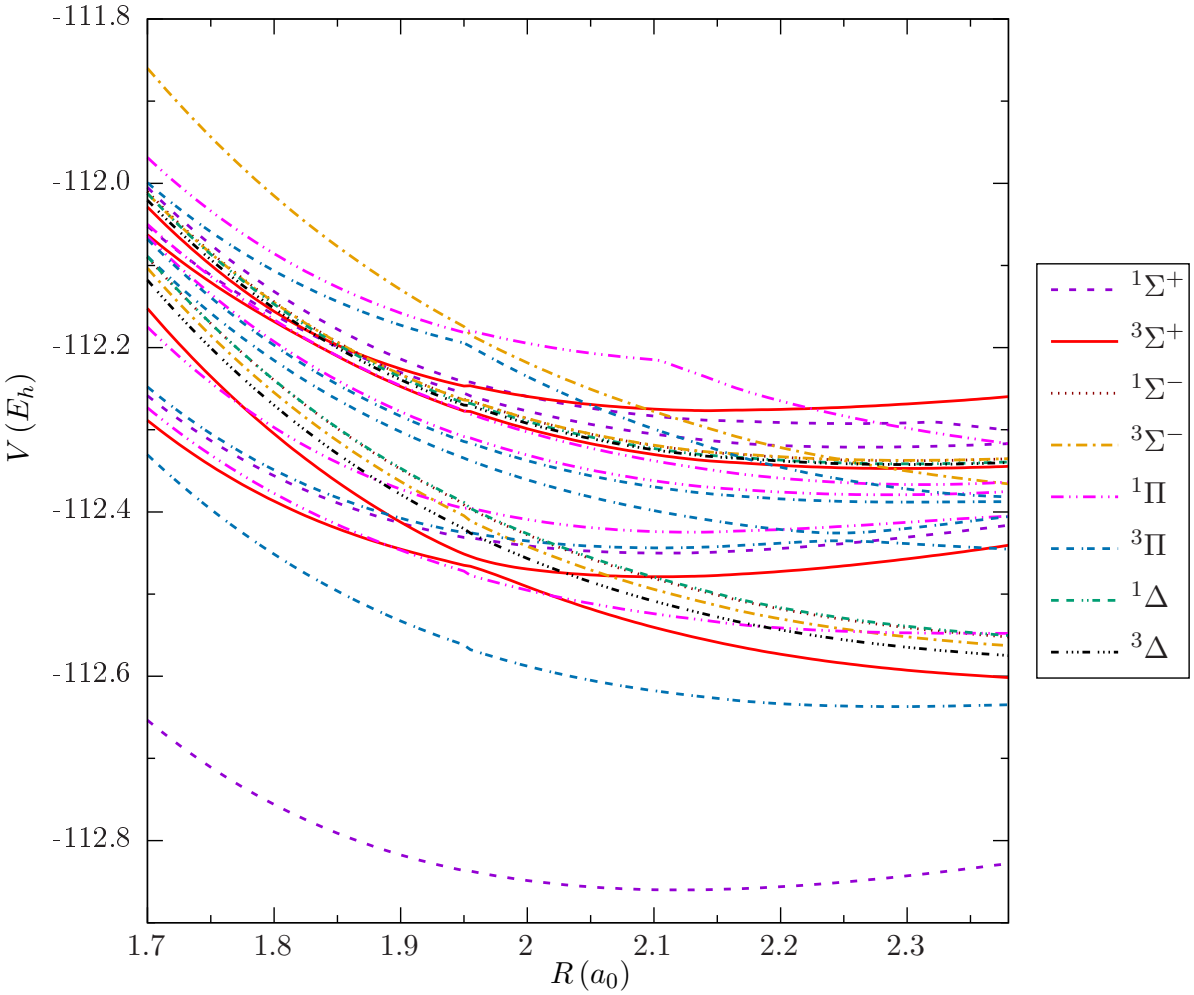

Figure 1. Calculated CASSCF potential energy curves for the 27 excited states of CO.

Table 2. Positions (E_r) and widths (Γ) of resonances detected for CO at its equilibrium geometry, $R_{eq} = 2.1323$ a$_0$. All quantities are in eV.

Symmetry	$E_r(\Gamma)$	comment
$1\,^2\Pi$	1.8744 (1.2916)	$X\,^1\Sigma^+$ Shape resonance
$1\,^2\Sigma^+$	10.1019 (0.1126)	Parent: $a'\,^3\Sigma^+$ / $b\,^3\Sigma^+$
$2\,^2\Sigma^+$	10.3850 (0.00049)	Parent: $b\,^3\Sigma^+$
$3\,^2\Sigma^+$	11.1579 (0.0048)	Parent: $B\,^1\Sigma^+$ and $2\,^3\Pi$
$2\,^2\Pi$		Parent: $A\,^1\Pi$
$3\,^2\Pi$		Parent: $3\,^3\Pi$
$4\,^2\Pi$	12.8306 (0.0889)	Parent: $4\,^3\Pi$ and $3\,^1\Pi$
$5\,^2\Pi$		Parent: $4\,^1\Pi$ and $3\,^3\Sigma^+$
$1\,^2\Delta$	13.3135 (0.1641)	Parent: $4\,^3\Pi$ and $3\,^1\Pi$

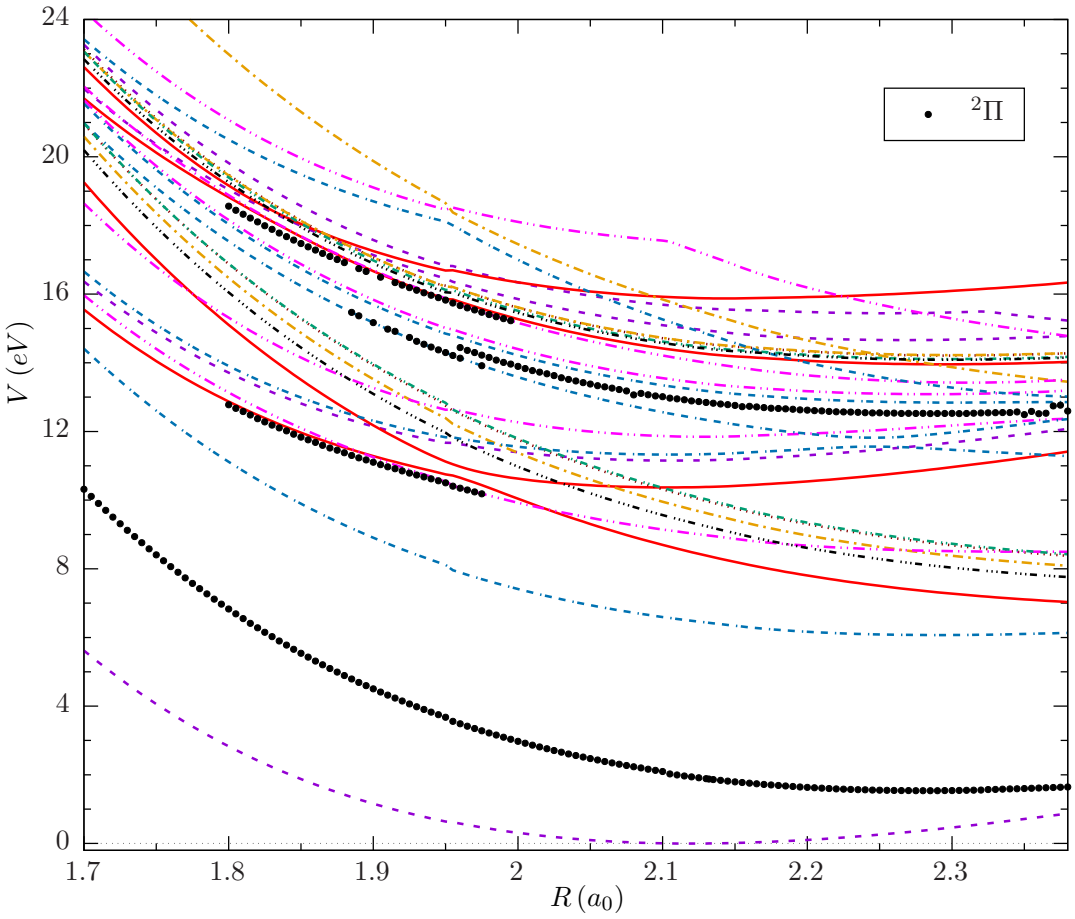

Figure 2. Calculated CO^- $^2\Pi$ symmetry resonance curves. Also shown are the CO target states, see Fig. 1 for specifications of these states. All energies are given relative to the minimum of the X $^1\Sigma^+$ CO ground state.

potential curves that run parallel to each other at the geometries of interest. The $^2\Delta$ can couple to both states via a p-wave and it is therefore reasonable to assume that these two states are joint parents. Conversely, the lowest 1 $^2\Sigma^+$ resonance appears to swap parents as function of internuclear separation: at short R it follows the $a'\,^3\Sigma^+$ curve which undergoes an avoided crossing with the $b\,^3\Sigma^+$ curve at about 1.96 a_0 with the resonance following the lower curve and then after this curve crosses the $b\,^3\Sigma^+$ curve at about 2.0 a_0, it follows the $b\,^3\Sigma^+$ curve. This parent swapping behaviour has previously been found in H_2^- Feshbach resonances (Stibbe & Tennyson 1997*b*). Similarly the second $^2\Sigma^+$ resonance apparently disappears in the region of the same curve crossing. While this may be caused by the resonance becoming so weakly bound that our calculations failed to identify, the disappearance of resonances in such circumstance has been noted before (Stibbe & Tennyson 1998).

One reason for identifying the resonance parent states is that it allows an accurate position for each resonance to be determined even though the target calculation necessarily only gives approximate target curves. This is because the binding energy of a given resonance to its parent state is usually both small and appropriately constant

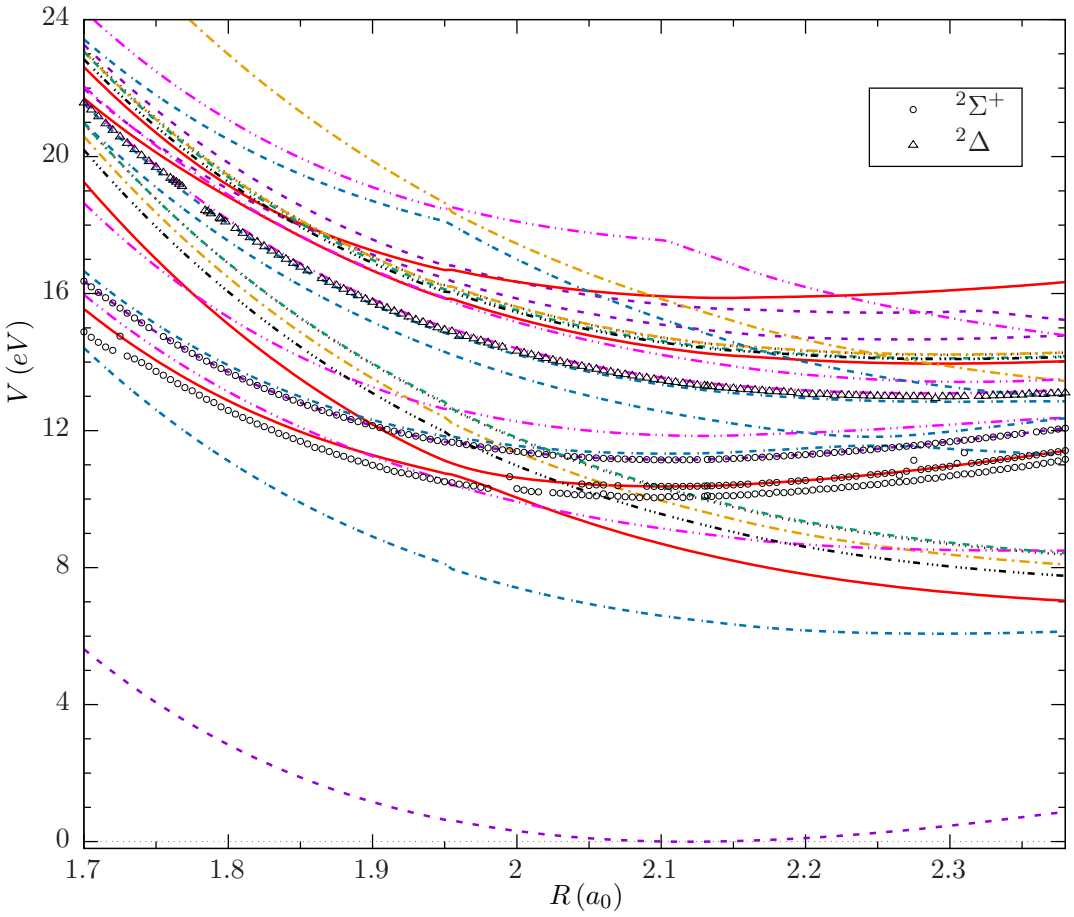

Figure 3. Calculated CO^- $^2\Sigma^+$ and $^2\Delta$ resonance curves. Also shown the CO target states, see Fig. 1 for specifications of these states. All energies are given relative to the minimum of the X $^1\Sigma^+$ CO ground state.

as a function of R. This means that the main error in the resonance position arises from the target calculation and, if improved target energies are known, it is possible to adjust the resonance curve accordingly (Stibbe & Tennyson 1997*a*).

Figures 4, 5 and 6 gives our resonance widths for the eight CO^- resonances we identified and the lowest $^2\Pi$ shape resonance. The widths appear more structured than the resonance positions. There are a number of reasons for this. Resonance widths are very sensitive to details of the physics and experience shows that fitting is very robust in determining resonance positions but widths are sensitive to precise details of the fit. In order to obtain the resonance positions and widths as accurately as possible we performed outer region calculations on very fine energy grids close to each resonance. The number of energy grid points, grid size and the starting energy input required for each of these was estimated by looking at eigenphase plots of the standard set of initial calculations performed on 0.1 a_0 R grid. Moreover, for this initial set of calculations the resonance parameters were determined by using both Breit-Wigner fits to the eigenphase sums (Tennyson & Noble 1984) and the time delays (Little et al. 2017) method; both these methods generally gave results close to each other. Therefore, for the

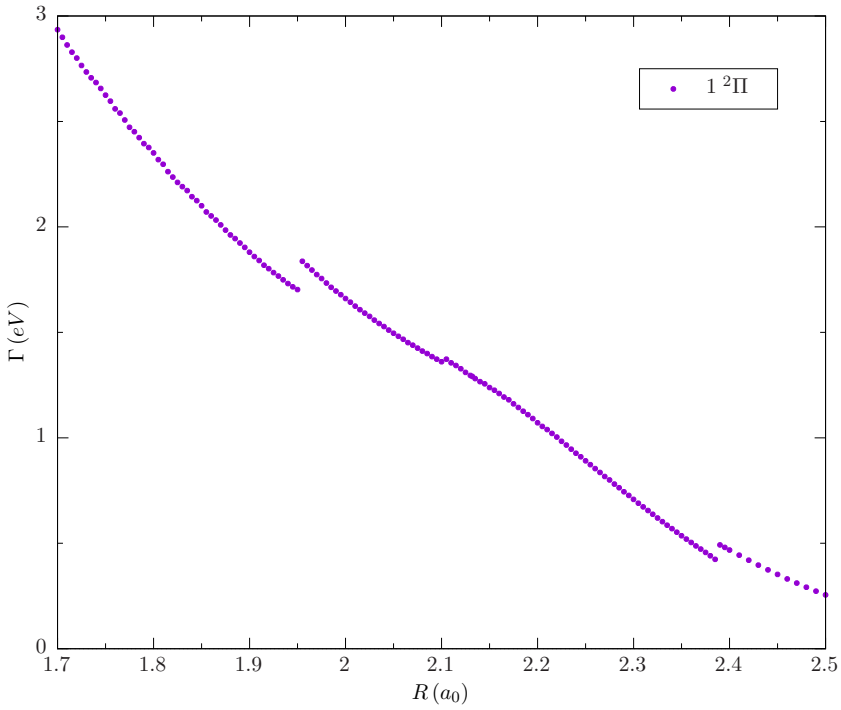

Figure 4. Calculated CO^- resonance widths (Γ) as a function of internuclear separation for the low-lying $^2\Pi$ shape resonance.

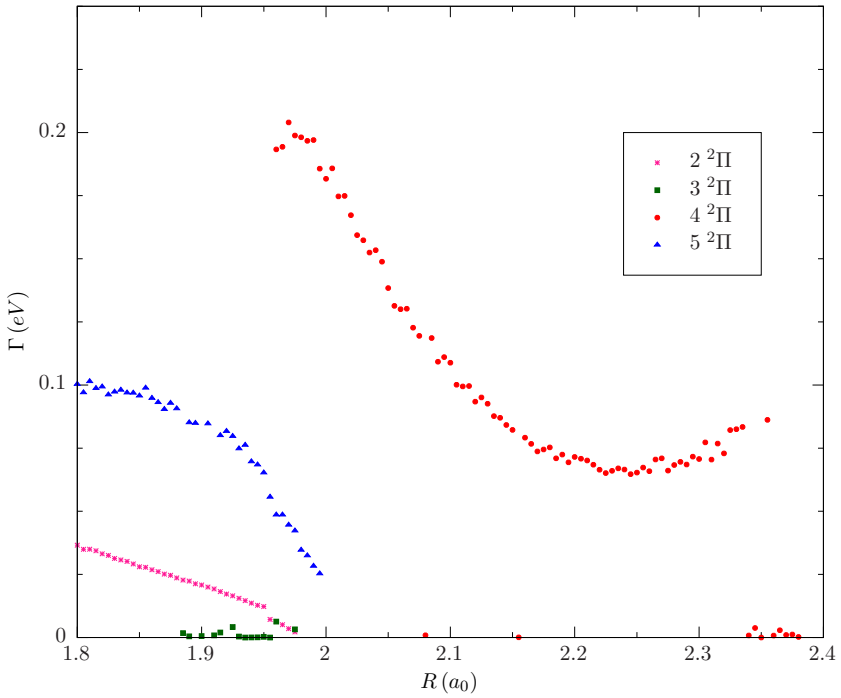

Figure 5. Calculated CO^- resonance widths (Γ) as a function of internuclear separation for the higher $^2\Pi$ resonances.

later calculations in finer R grid only the eigenphase sums fitting method was used. At some of geometries the eigenphase sum fitting code (RESON) found multiple resonances

some of which looked to be spurious, in such cases we picked the ones by looking at the eigenphase sum and cross section plots as well as tracing the continuity of resonance positions as function of R.

Figures 4, 5 and 6 show pronounced structures in the resonance widths. Some of these occur naturally due to crossings of the target curves and associated changes in parantage; some of the structure is undoubtedly an artifact of our calculation. As shown in Fig. 4, the width of the $^2\Pi$ shape resonance drop almost monotonically with R; it become 0.11 eV at $R = 2.6$ a$_0$ and goes to zero as the anion state becomes bound relative the X $^1\Sigma^+$ ground state of CO at $R \approx 2.7$ a$_0$. The curve, however, shows two jumps in these widths. These jumps are probably numerical, for example the structure at $R = 1.95$ a$_0$ appears to be associated with slight discontinuities in the in the underlying target electronic structure calculations at this geometry, rather than being due to any underlying physics of the problem. However, the jumps are relatively small and well within the uncertainty with which our calculation predicts this width. Conversely, there is pronounced structure in the 1 $^2\Sigma^+$ resonance width at about $R = 2$ a$_0$, see Fig. 6; this occurs where the parent $a'\,^3\Sigma^+$ and $b\,^3\Sigma^+$ states cross. The other variations are probably due to issues in performing fits for a narrow resonance close to a target curve. The structure in this resonance at short bondlengths is probably due to another curve cross although the density of target curves in this region makes it difficult to be definitive about which curves are involved. Similarly the structure in the width of the $^1\Delta$ resonance at $R < 1.8$ a$_0$, also shown in Fig. 6, is almost certainly associated with changes in target curves in this region, but the density of curves is such that it is difficult to be precise about this. The widths of the two very narrow resonances, the second and third $^2\Sigma^+$ states, appear considerably busier. While some of this structure is also likely to be associated with changes in the target curves, the act of fitting leads to small differences in the widths which are exaggerated by the fact that these widths are magnified on the plot.

4. Conclusion

While it seems likely that many (maybe nearly all) molecules support multiple Feshbach resonances in the energy region just below the ionisation threshold; however, these have only been systematically characterised theoretically the electron – H_2 system (Stibbe & Tennyson 1998). Here we present the first successful *ab initio* characterisation of CO resonances in the 10 to 14 eV region. These resonances are well-known from experimental studies and dissociative electron attachment (DEA) experiments have provided detailed insights into them. We find a significant number of narrow resonances, three $^2\Sigma^+$, four $^2\Pi$ and one $^2\Delta$, in the 10 – 14 eV region, as well as, of course, the broad low-lying $^2\Pi$ shape resonance. We have characterised the complex resonance potential energy curves (i.e., the positions and widths) for all these anion states as a function of internuclear separation. There are too many of these curves to make a direct association between individual resonance curves and particular dissociative electron attachment (DEA)

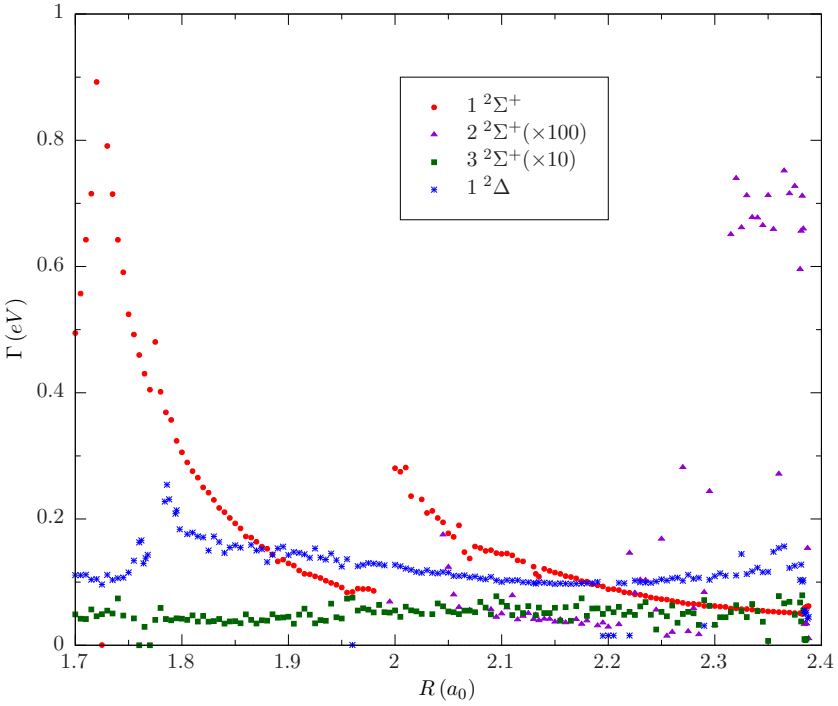

Figure 6. Calculated CO^- resonance widths (Γ) as a function of internuclear separation for the non-$^2\Pi$ resonances.

features. Theoretically, the next step is to use these complex resonance potential energy curves as input for DEA calculations. Similar studies have already been successfully performed for the 10 – 14 eV Feshbach H_2^- resonances (Celiberto et al. 2012, Celiberto et al. 2013). To facilitate such calculations we provide our numerical values for the potential energy curves of our 27 target states and complex potential energy curves (positions and widths) for the 9 resonances we identify as supplementary data to this article.

Acknowledgment

AD gratefully acknowledges SERB, Govt. of India (grant number: EMR/2017/003179). We thank Kalyan Chakrabarti and Vincenzo Laporta for helpful discussions.

References

Allan M 1989 *J. Electron Spectrosc. Related Phenom.* **48**, 219 – 351.
Allan M 2010 *Phys. Rev. A* **81**, 042706.
Cadex I, Tronc M & Hall R I 1975 *J. Phys. B: At. Mol. Opt. Phys.* **8**, L73–L76.
Campbell L, Allan M & Brunger M J 2011 *J. Geophys. Res.* **116**, A09321.
Carr J M, Galiatsatos P G, Gorfinkiel J D, Harvey A G, Lysaght M A, Madden D, Mašín Z, Plummer M, Tennyson J & Varambhia H N 2012 *Eur. Phys. J. D* **66**, 58.
Celiberto R, Janev R K, Laporta V, Tennyson J & Wadehra J M 2013 *Phys. Rev. A* **88**, 062701.
Celiberto R, Janev R K, Wadehra J M & Tennyson J 2012 *Chem. Phys.* **398**, 206–213.

Chantry P J 1968 *Phys. Rev.* **172**, 125.
Dora A, Bryjko L, van Mourik T & Tennyson J 2009 *J. Chem. Phys.* **130**, 164307.
Dora A & Tennyson J 2019 *in* P. C Deshmukh, E Krishnakumar, S Fritzsche, M Krishnamurthy & S Majumder, eds, 'Quantum Collisions and Confinement of Atomic and Molecular Species, and Photons' Vol. 230 Springer Singapore Singapore pp. 48–59.
Dora A, Tennyson J & Chakrabarti K 2016 *Eur. Phys. J. D* **70**, 197.
Fabrikant I I, Eden S, Mason N J & Fedor J 2017 *Adv. At. Mol. Opt. Phys.* **66**, 545–657.
Faure A, Gorfinkiel J D, Morgan L A & Tennyson J 2002 *Comput. Phys. Commun.* **144**, 224–241.
Gibson J C, Morgan L A, Gulley R J, Brunger M J, Bundschu C T & Buckman S J 1996 *J. Phys. B: At. Mol. Opt. Phys.* **29**, 3197–3214.
Gope K, Tadsare V, Prabhudesai V S, Mason N J & Krishnakumar E 2016 *Eur. Phys. J. D* **70**, 134.
Gorfinkiel J D, Morgan L A & Tennyson J 2002 *J. Phys. B: At. Mol. Opt. Phys.* **35**, 543–555.
Haddad G N & Milloy H B 1983 *Austrialian J. Phys.* **36**, 473–484.
Hall R I, Cadex I, Schermann C & Tronc M 1977 *Phys. Rev. A* **15**, 599–610.
Laporta V, Cassidy C M, Tennyson J & Celiberto R 2012 *Plasma Sources Sci. Technol.* **21**, 045005.
Little D A, Tennyson J, Plummer M & Sunderland A 2017 *Comput. Phys. Commun.* **215**, 137–148.
Mašín Z, Benda J, Gorfinkiel J D, Harvey A G & Tennyson J 2020 *Comput. Phys. Commun.* **249**, 107092.
Mazeau J, Gresteau F, Joyez G, Reinhardt J & Hall R I 1972 *J. Phys. B: At. Mol. Phys.* **5**, 1890.
Mazeau J, Schermann C & Joyez G 1975 *J. Electron Spectrosc. Related Phenomena* **7**, 269 – 279.
Meltzer T, Tennyson J, Mašín Z, Zammit M C, Scarlett L H, Fursa D V & Bray I 2020 *J. Phys. B: At. Mol. Opt. Phys.* .
Middleton A G, Brunger M J & Teubner P J O 1993 *J. Phys. B: At. Mol. Opt. Phys.* **26**, 1743.
Morgan L A & Tennyson J 1993 *J. Phys. B: At. Mol. Opt. Phys.* **26**, 2429–2441.
Morgan L A, Tennyson J & Gillan C J 1998 *Comput. Phys. Commun.* **114**, 120–128.
Nag P & Nandi D 2015*a* *Phys. Rev. A* **91**, 056701.
Nag P & Nandi D 2015*b* *Phys. Chem. Chem. Phys.* **17**, 7130–7137.
Newman D S, Zubek M & King G C 1983 *J. Phys. B: At. Mol. Opt. Phys.* **16**, 2247.
Nielsen E S, Jørgensen P & Oddershede J 1980 *J. Chem. Phys.* **73**, 6238.
Olszewski R, Woliński P & Zubek M 1998 *Chem. Phys. Lett.* **297**, 537 – 542.
Pearson P K & Lefebvre-Brion H 1976 *Phys. Rev. A* **13**, 2106–2113.
Polley J P & Bailey T L 1988 *Phys. Rev. A* **37**, 733–736.
Poparić G B, Belić D S & Vicić M D 2006 *Phys. Rev. A* **73**, 062713.
Rapp D & Briglia D D 1965 *J. Chem. Phys.* **43**, 1480–1489.
Salvini S, Burke P G & Noble C J 1984 *J. Phys. B: At. Mol. Opt. Phys.* **17**, 2549.
Sanche L & Schulz G J 1971 *Phys. Rev. Lett.* **26**, 943–946.
Schulz G J 1973 *Rev. Mod. Phys.* **45**, 423–486.
Stamatovic A & Schulz G J 1970 *J. Chem. Phys.* **53**, 2663–2667.
Stibbe D T & Tennyson J 1997*a* *Phys. Rev. Lett.* **79**, 4116–4119.
Stibbe D T & Tennyson J 1997*b* *J. Phys. B: At. Mol. Opt. Phys.* **30**, L301–L307.
Stibbe D T & Tennyson J 1998 *J. Phys. B: At. Mol. Opt. Phys.* **31**, 815–844.
Tennyson J 2010 *Phys. Rep.* **491**, 29–76.
Tennyson J & Noble C J 1984 *Comput. Phys. Commun.* **33**, 421–424.
Tian S X, Wu B, Xia L, Wang Y F, Li H K, Zeng X J, Luo Y & Yang J 2013 *Phys. Rev. A* **88**, 012708.
Wallbank B, Daviel S, Comer J & Hickes P 1983 *J. Phys. B: At. Mol. Phys.* **16**, 3065–3076.
Wang X D, Xuan C J, Luo Y & Tian S X 2015 *J. Chem. Phys.* **143**, 066101.
Weatherford C A & Huo W M 1990 *Phys. Rev. A* **41**, 186–197.
Werner H J, Knowles P J, Knizia G, Manby F R & Schütz M 2012 *WIREs Comput. Mol. Sci.* **2**, 242–253.
Zawadzki M, Khakoo M A, Voorneman L, Ratkovic L, Mašín Z, Houfek K, Dora A & Tennyson J 2020 *J. Phys. B: At. Mol. Opt. Phys.* .